

Resonance capture cross section of  $^{207}\text{Pb}$ 

C. Domingo-Pardo<sup>1,2\*</sup>, U. Abbondanno<sup>3</sup>, G. Aerts<sup>4</sup>, H. Álvarez-Pol<sup>5</sup>, F. Alvarez-Velarde<sup>6</sup>, S. Andriamonje<sup>4</sup>, J. Andrzejewski<sup>7</sup>, P. Assimakopoulos<sup>8</sup>, L. Audouin<sup>2</sup>, G. Badurek<sup>9</sup>, P. Baumann<sup>10</sup>, F. Bečvář<sup>11</sup>, E. Berthoumieux<sup>4</sup>, S. Bisterzo<sup>12,2</sup>, F. Calviño<sup>13</sup>, D. Cano-Ott<sup>6</sup>, R. Capote<sup>14,15</sup>, C. Carrapiço<sup>16</sup>, P. Cennini<sup>17</sup>, V. Chepel<sup>18</sup>, E. Chiaveri<sup>17</sup>, N. Colonna<sup>19</sup>, G. Cortes<sup>13</sup>, A. Couture<sup>20</sup>, J. Cox<sup>20</sup>, M. Dahlfors<sup>17</sup>, S. David<sup>21</sup>, I. Dillman<sup>2</sup>, R. Dolfini<sup>22</sup>, W. Dridi<sup>4</sup>, I. Duran<sup>5</sup>, C. Eleftheriadis<sup>23</sup>, M. Embid-Segura<sup>6</sup>, L. Ferrant<sup>21</sup>, A. Ferrari<sup>17</sup>, R. Ferreira-Marques<sup>18</sup>, L. Fitzpatrick<sup>17</sup>, H. Fraiss-Koelbl<sup>14</sup>, K. Fujii<sup>3</sup>, W. Furman<sup>24</sup>, R. Gallino<sup>12</sup>, I. Goncalves<sup>18</sup>, E. Gonzalez-Romero<sup>6</sup>, A. Goverdovski<sup>25</sup>, F. Gramegna<sup>26</sup>, E. Griesmayer<sup>14</sup>, C. Guerrero<sup>6</sup>, F. Gunsing<sup>4</sup>, B. Haas<sup>27</sup>, R. Haight<sup>28</sup>, M. Heil<sup>2</sup>, A. Herrera-Martinez<sup>17</sup>, M. Igashira<sup>29</sup>, S. Isaev<sup>21</sup>, E. Jericha<sup>9</sup>, Y. Kadi<sup>17</sup>, F. Käppeler<sup>2</sup>, D. Karamanis<sup>8</sup>, D. Karadimos<sup>8</sup>, M. Kerveno<sup>10</sup>, V. Ketlerov<sup>25,17</sup>, P. Koehler<sup>30</sup>, V. Konovalov<sup>24,17</sup>, E. Kossionides<sup>31</sup>, M. Krčička<sup>11</sup>, C. Lamboudis<sup>8</sup>, H. Leeb<sup>9</sup>, A. Lindote<sup>18</sup>, I. Lopes<sup>18</sup>, M. Lozano<sup>15</sup>, S. Lukic<sup>10</sup>, J. Marganec<sup>7</sup>, S. Marrone<sup>19</sup>, P. Mastinu<sup>26</sup>, A. Mengoni<sup>14,17</sup>, P.M. Milazzo<sup>3</sup>, C. Moreau<sup>3</sup>, M. Mosconi<sup>2</sup>, F. Neves<sup>18</sup>, H. Oberhummer<sup>9</sup>, M. Oshima<sup>32</sup>, S. O'Brien<sup>20</sup>, J. Pancin<sup>4</sup>, C. Papachristodoulou<sup>8</sup>, C. Papadopoulos<sup>33</sup>, C. Paradela<sup>5</sup>, N. Patronis<sup>8</sup>, A. Pavlik<sup>34</sup>, P. Pavlopoulos<sup>35</sup>, L. Perrot<sup>4</sup>, R. Plag<sup>2</sup>, A. Plompen<sup>36</sup>, A. Plukis<sup>4</sup>, A. Poch<sup>13</sup>, C. Pretel<sup>13</sup>, J. Quesada<sup>15</sup>, T. Rauscher<sup>37</sup>, R. Reifarth<sup>28</sup>, M. Rosetti<sup>38</sup>, C. Rubbia<sup>22</sup>, G. Rudolf<sup>10</sup>, P. Rullhusen<sup>36</sup>, J. Salgado<sup>16</sup>, L. Sarchiapone<sup>17</sup>, I. Savvidis<sup>23</sup>, C. Stephan<sup>21</sup>, G. Tagliente<sup>19</sup>, J.L. Tain<sup>1</sup>, L. Tassan-Got<sup>21</sup>, L. Tavora<sup>16</sup>, R. Terlizzi<sup>19</sup>, G. Vannini<sup>39</sup>, P. Vaz<sup>16</sup>, A. Ventura<sup>38</sup>, D. Villamarin<sup>6</sup>, M. C. Vicente<sup>6</sup>, V. Vlachoudis<sup>17</sup>, R. Vlastou<sup>33</sup>, F. Voss<sup>2</sup>, S. Walter<sup>2</sup>, H. Wendl<sup>17</sup>, M. Wiescher<sup>20</sup>, K. Wisshak<sup>2</sup>

## The n\_TOF Collaboration

<sup>1</sup>*Instituto de Física Corpuscular, CSIC-Universidad de Valencia, Spain*

<sup>2</sup>*Forschungszentrum Karlsruhe GmbH (FZK), Institut für Kernphysik, Germany*

<sup>3</sup>*Istituto Nazionale di Fisica Nucleare, Trieste, Italy*

<sup>4</sup>*CEA/Saclay - DSM, Gif-sur-Yvette, France*

<sup>5</sup>*Universidad de Santiago de Compostela, Spain*

<sup>6</sup>*Centro de Investigaciones Energeticas Medioambientales y Tecnológicas, Madrid, Spain*

<sup>7</sup>*University of Lodz, Lodz, Poland*

<sup>8</sup>*University of Ioannina, Greece*

<sup>9</sup>*Atominstytut der Österreichischen Universitäten, Technische Universität Wien, Austria*

<sup>10</sup>*Centre National de la Recherche Scientifique/IN2P3 - IReS, Strasbourg, France*

<sup>11</sup>*Charles University, Prague, Czech Republic*

<sup>12</sup>*Dipartimento di Fisica Generale, Università di Torino, Italy*

<sup>13</sup>*Universitat Politècnica de Catalunya, Barcelona, Spain*

<sup>14</sup>*International Atomic Energy Agency, NAPC-Nuclear Data Section, Vienna, Austria*

<sup>15</sup>*Universidad de Sevilla, Spain*

<sup>16</sup>*Instituto Tecnológico e Nuclear (ITN), Lisbon, Portugal*

<sup>17</sup>*CERN, Geneva, Switzerland*

<sup>18</sup>*LIP - Coimbra & Departamento de Física da Universidade de Coimbra, Portugal*

<sup>19</sup>*Istituto Nazionale di Fisica Nucleare, Bari, Italy*

<sup>20</sup>*University of Notre Dame, Notre Dame, USA*

<sup>21</sup>*Centre National de la Recherche Scientifique/IN2P3 - IPN, Orsay, France*

<sup>22</sup>*Università degli Studi Pavia, Pavia, Italy*

<sup>23</sup>*Aristotle University of Thessaloniki, Greece*

<sup>24</sup>*Joint Institute for Nuclear Research, Frank Laboratory of Neutron Physics, Dubna, Russia*

<sup>25</sup>*Institute of Physics and Power Engineering, Kaluga region, Obninsk, Russia*

<sup>26</sup>*Istituto Nazionale di Fisica Nucleare (INFN), Laboratori Nazionali di Legnaro, Italy*

<sup>27</sup>*Centre National de la Recherche Scientifique/IN2P3 - CENBG, Bordeaux, France*

<sup>28</sup>*Los Alamos National Laboratory, New Mexico, USA*

<sup>29</sup>*Tokyo Institute of Technology, Tokyo, Japan*

<sup>30</sup>*Oak Ridge National Laboratory, Physics Division, Oak Ridge, USA*

<sup>31</sup>*NCSR, Athens, Greece*

<sup>32</sup>*Japan Atomic Energy Research Institute, Tokai-mura, Japan*

<sup>33</sup>*National Technical University of Athens, Greece*

<sup>34</sup>*Institut für Isotopenforschung und Kernphysik, Universität Wien, Austria*

<sup>35</sup>*Pôle Universitaire Léonard de Vinci, Paris La Défense, France*

<sup>36</sup>*CEC-JRC-IRMM, Geel, Belgium*

<sup>37</sup>*Department of Physics and Astronomy - University of Basel, Basel, Switzerland*

<sup>38</sup>*ENEA, Bologna, Italy*

<sup>39</sup>*Dipartimento di Fisica, Università di Bologna, and Sezione INFN di Bologna, Italy*

(Dated: July 6, 2018)

The radiative neutron capture cross section of  $^{207}\text{Pb}$  has been measured at the CERN neutron time of flight installation n\_TOF using the pulse height weighting technique in the resolved energy region. The measurement has been performed with an optimized setup of two  $\text{C}_6\text{D}_6$  scintillation detectors, which allowed us to reduce scattered neutron backgrounds down to a negligible level. Resonance parameters and radiative kernels have been determined for 16 resonances by means of an R-matrix analysis in the neutron energy range from 3 keV to 320 keV. Good agreement with previous measurements was found at low neutron energies, whereas substantial discrepancies appear beyond 45 keV. With the present results, we obtain an  $s$ -process contribution of  $77\pm 8\%$  to the solar abundance of  $^{207}\text{Pb}$ . This corresponds to an  $r$ -process component of  $23\pm 8\%$ , which is important for deriving the U/Th ages of metal poor halo stars.

PACS numbers: 25.40.Lw, 27.80.+w, 97.10.Cv

## I. INTRODUCTION

Since  $^{207}\text{Pb}$  is one of the final products of the Th/U  $\alpha$ -decay chains, its abundance provides a constraint for the Th/U abundances and their use as cosmochronometer [1]. The  $s$  abundance of  $^{207}\text{Pb}$  has been shown to depend only weakly on details of stellar  $s$ -process models [2] so that the  $r$  component can be reliably determined by subtraction from the solar value,  $N_r = N_\odot - N_s$ .

Apart from its astrophysical importance, the neutron capture cross section of this isotope is also of relevance for the design of fast reactor systems. An eutectic mixture of Pb/Bi is presently considered as an appropriate spallation target and coolant for accelerator driven systems [3]. Because 22.1% of natural lead consists of  $^{207}\text{Pb}$ , the relatively large neutron capture cross section of this isotope affects the neutron balance, and is therefore important for the design of this type of hybrid reactors.

Given the large neutron scattering width in some of the  $^{207}\text{Pb}$  resonances, the neutron sensitivity of the detector system becomes instrumental for the effective reduction of backgrounds due to scattered neutrons. For this reason an optimized setup based on  $\text{C}_6\text{D}_6$  detectors has been employed by the n\_TOF collaboration, well suited for the subsequent application of the pulse height weighting technique (PHWT), which was used in data analysis (Sec. III). With the adopted experimental setup angular distribution effects of the primary  $\gamma$  radiation emitted for neutron capture events with orbital angular momentum  $l > 0$  are important. This effect, which is large for some resonances, could be properly treated in the data analysis as described in Section III. The resulting neutron capture cross section is presented in Section IV, and the astrophysical implications of this measurement are summarized in Section V.

## II. EXPERIMENT

The measurement was performed with an enriched sample in the form of a metal disk 20 mm in diameter and 2 mm in thickness, containing 92.40% of  $^{207}\text{Pb}$ , 5.48% of  $^{208}\text{Pb}$  and 2.12% of  $^{206}\text{Pb}$ . The sample was mounted in vacuum inside a sample changer made from carbon fiber together with a gold sample for absolute cross section normalization. In addition, a  $^{208}\text{Pb}$  sample was used to study the background coming from in-beam  $\gamma$  rays, which are scattered by the sample. The long flight path of 185.2 m and the short proton pulse width of 6 ns (RMS) are the important properties for achieving the high resolution in time-of-flight (TOF) characteristic of the n\_TOF spallation source [4].

Neutron capture events were registered via the prompt capture  $\gamma$ -ray cascade by a set of two  $\text{C}_6\text{D}_6$  detectors, which were optimized with respect to neutron sensitivity [5]. The detectors were placed at  $\sim 125^\circ$  with respect to the incident neutron beam in order to minimize angular distribution effects of the emitted capture radiation. A schematic view of the experimental setup can be seen in Fig. 2 of Ref. [6]. In this configuration, the in-beam  $\gamma$ -ray background was also substantially reduced.

The neutron flux was monitored by means of a  $200 \mu\text{g}/\text{cm}^2$  thick  $^6\text{Li}$ -foil mounted 3 m upstream of the  $^{207}\text{Pb}$  sample. Particles from  $^6\text{Li}(n, \alpha)^3\text{H}$  reactions are registered with four silicon detectors surrounding the  $^6\text{Li}$ -foil outside of the beam [7].

The saturated resonance technique [8] using the 4.9 eV  $^{197}\text{Au}$  resonance was applied for absolute calibration of the  $^{207}\text{Pb}$  capture yield. Calibration of the yield in this way requires the precise knowledge of the neutron intensity versus the neutron energy. This has been determined with an uncertainty of 2% [9] by two independent measurements performed with the  $^6\text{Li}$  monitor described before and with a calibrated fission chamber [10].

## III. CAPTURE DATA ANALYSIS

The first aspect of the data analysis obviously concerns the determination of the weighting function (WF). Based on previous experience, the WF for the measured samples of  $^{197}\text{Au}$  (used for normalization) and of  $^{207}\text{Pb}$  was

---

\*Corresponding author, address: Apdo. Correos 22085, 46071 Valencia (Spain). Tel.: +34963543499, e-mail cesar.domingo.pardo@cern.ch.

calculated via the Monte Carlo technique. The procedure followed has been described in detail in Refs. [11, 12].

The capture  $\gamma$ -ray spectra of both samples were calculated with a Monte Carlo code in order to estimate the corresponding uncertainty of the WF, which turned out to be less than 0.5%. It has been experimentally demonstrated [12] that the combination of WFs obtained by the Monte Carlo method with the saturated resonance technique yields an overall systematic uncertainty of better than 3%. However, this level of accuracy can be only achieved if all sources of systematic uncertainty are properly taken into account. This refers mainly to (i) the determination of the neutron flux, (ii) the treatment of the background components, and (iii) the effect of the electronic threshold used for the signals from the  $C_6D_6$  detectors. In the particular case of  $^{207}\text{Pb}$ , one has to consider also a pronounced angular distribution effect of the capture  $\gamma$  rays due to the low multiplicity in the de-excitation pattern of  $^{208}\text{Pb}$ . This effect will be considered separately since it depends strongly on the resonance spin and parity ( $J^\pi$ ).

The various sources of systematic uncertainty are listed in Table I. In the following, the treatment of these effects is described in detail.

TABLE I: Systematic effects and related uncertainties.

Effect	Uncertainty (in %)
Weighting function, saturated resonance technique and electronic threshold	<2
Background determination	<0.5 (1.5) <sup>a</sup>
Energy-dependence of neutron flux	2
Neutron sensitivity	<0.3
Angular distribution: for $J^\pi=1^+$	0.6 (8) <sup>b</sup>
for $J^\pi=2^+$	0.3

<sup>a</sup> Broad  $s$ -wave resonances at  $E_o = 41$  and 256 keV (see also Table II). <sup>b</sup> Resonances with unknown angular distribution.

### A. Background

In the present measurement the background in the resolved resonance region (RRR) is dominated by delayed  $\gamma$ -rays accompanying the neutron beam and scattered in the sample. These  $\gamma$ -rays arise essentially from neutron capture in the water moderator of the n\_TOF spallation target and exhibit a smooth dependence on neutron time of flight. For samples of equal atomic number  $Z$  and similar thickness the background level is also very similar. Since all observed resonances in  $^{207}\text{Pb}$  were well isolated, the background level was best determined by choosing a relatively wide neutron energy window around each resonance and defining the background level by a constant term. The neutron energy dependence of the background level fitted for each resonance was afterwards cross checked with a measurement of a  $^{208}\text{Pb}$  sample. The  $^{208}\text{Pb}$  sample itself showed very few resonances in the entire energy region and was, therefore, well suited

for determination of the background from in-beam  $\gamma$  rays. The respective systematic uncertainties were less than 1.5% for the broad resonances at 41 and 256 keV, and below 0.5% for all the others.

A different type of background might arise in the measurement of resonances that show a dominant scattering channel like the  $s$ - and  $p$ -wave resonances at 41 keV and 128 keV (Table II), where  $\Gamma_n/\Gamma_\gamma \approx 300$ . Thanks to the optimized detection setup and the small amount of material around the sample and the detectors, this background turned out to be negligible in the present measurement.

### B. Electronic threshold

The low energy cut-off in the pulse height spectra due to the electronic threshold ( $\approx 340$  keV in this measurement) had a non-negligible influence on the yield measured with the  $\gamma$ -ray detectors. The effect can be corrected by modeling the capture cascades with a Monte Carlo simulation of the complete pulse height spectra recorded in the n\_TOF detection system as described in Refs. [9, 11, 12].

Following neutron captures on  $^{207}\text{Pb}$ , the de-excitation pattern of the  $^{208}\text{Pb}$  resonances is rather simple. It basically consists of a single  $\gamma$ -transition of 7.37 MeV for  $J = 1$  and of a two-step cascade in case of  $J = 2$  resonances [13, 14]. Therefore, the Monte Carlo simulations of the capture spectra and the estimate of the threshold effect are correspondingly straightforward and reliable, yielding correction factors of  $5\pm 1\%$  and  $4\pm 1\%$  for  $J = 1$  and  $J = 2$  resonances, respectively.

### C. Angular distribution effects

The low multiplicity ( $m = 1$  for  $J = 1$  and  $m = 1-2$  for  $J = 2$  resonances) of the  $^{207}\text{Pb}$  capture cascades has the experimental disadvantage that it causes strong angular distribution effects in the measured pulse height spectra. Indeed, captures with orbital angular momenta  $l > 0$  lead to aligned states in the compound nucleus, perpendicular to the incident neutron beam. This causes anisotropy in the angular distribution of the prompt  $\gamma$  rays,

$$W(\theta) = \sum_k A_k P_k(\cos\theta) = 1 + A_2 P_2(\cos\theta) + A_4 P_4(\cos\theta) + A_6 P_6(\cos\theta), \quad (1)$$

where  $P_k(\cos\theta)$  are the Legendre polynomials of order  $k$  and  $A_k$  are coefficients, which depend on the initial ( $J$ ) and final ( $J'$ ) spin values, on the multiplicities ( $L$ ) of the transition, and on the degree of alignment. With ideal  $\gamma$  detectors of negligible volume, this effect would be minimized by setting both detectors at  $125^\circ$ . However,

the  $C_6D_6$  detectors ( $\sim 1$  l volume) cover a substantial solid angle. Hence,  $\gamma$ -rays are registered in a relatively broad angular range around  $125^\circ$ .

For resonances with spin  $J^\pi = 1^+$  there is a channel spin admixture ( $s = 0, 1$ ), which contributes to an incomplete alignment with generally unknown proportions of the two channels with  $s = 0$  and  $s = 1$ . The  $A_k$  coefficients in Eq. 1 could be determined for the two  $1^+$  resonances at 30.5 keV and 37.7 keV (Table II) by means of measured angular distributions [15] and using the formulae in Ref.[16]. With this information the Monte Carlo simulations of the experimental setup yielded correction factors of  $f_{30\text{ keV}}^{\theta,1^+} = 0.965(3)$  and  $f_{37\text{ keV}}^{\theta,1^+} = 1.037(6)$  as described in detail in Ref. [9]. For the other three  $1^+$  resonances at 90 keV, 128 keV and 130 keV, where angular distributions are unknown, the corrections could not be determined. Instead, a systematic uncertainty of 8% was adopted in these cases. This value was estimated by means of Monte Carlo simulations of our experimental setup using different angular distributions, ranging from alignment zero up to total alignment.

For resonances with  $J^\pi=2^+$  the de-excitation occurs predominantly by emission of a two-step cascade [13]. The angular distribution of the first  $\gamma$ -ray can be calculated using the formulae in Ref. [16]. The angular distribution of the second  $\gamma$ -ray is influenced by the realignment introduced by the previous transition and it could be also calculated by modifying the formulae in Ref.[16]. The final yield correction factor for  $2^+$  resonances (considering also a 10% branching to the ground state) results in a value  $f^{\theta,2^+} = 1.015(3)$ .

#### D. R-matrix fits

The capture yield corrected for the effects described above,

$$f^t \times f^\theta \times Y^{exp} = B + Y(E_o, \Gamma_\gamma, \Gamma_n), \quad (2)$$

was analyzed by means of the R-matrix analysis code SAMMY [17].  $B$  is a constant term describing the background in the region of each resonance. In cases, where the neutron width  $\Gamma_n$  is well known from transmission measurements and considerably larger than the capture width  $\Gamma_\gamma$ ,  $\Gamma_n$  was kept fixed in our analysis. In other cases and where the number of counts in the resonance was sufficiently large, we preferred to vary  $\Gamma_n$  and  $\Gamma_\gamma$  in order to better describe the corresponding capture area or radiative kernel. Fig. 1 shows the measured capture yield for the two first resonances in  $^{207}\text{Pb}$ . The continuous line corresponds to an R-matrix fit performed with the SAMMY code.

## IV. RESULTS AND UNCERTAINTIES

The parameters and radiative kernels of the analyzed  $^{207}\text{Pb}$  resonances are summarized in Table II. Orbital

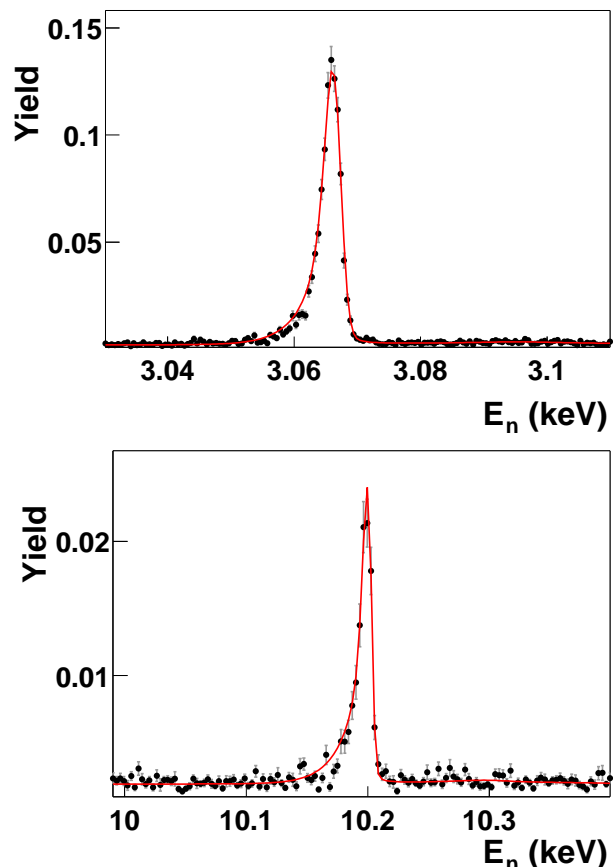


FIG. 1: (Color online) R-matrix fit for two of the resonances measured in this work at 3 keV and 10 keV.

angular momenta  $l$  and resonance spin  $J$  were taken from Ref. [18].

According to the discussion in the previous section, the radiative kernels can be given with an overall systematic uncertainty of  $\approx 3\%$ , except for the resonances at 90 keV, 128 keV and 130 keV with spin  $J = 1$ , where a systematic uncertainty of 8% had to be adopted (see Table I).

The radiative kernels (last column in Table II) are compared in Fig. 2 with previous measurements made at ORNL[13, 14].

For the first four resonances our results are in good agreement, whereas serious discrepancies appear at higher energy, mainly beyond 30 keV. It is remarkable that the radiative kernels of seven out of the nine  $J = 1$  resonances reported here are systematically smaller than those of Ref. [13], whereas the cross sections for  $J = 2$  resonances are in agreement or higher. Such discrepancies can not be explained only in terms of the experimental aspects discussed in the previous section, but must be due to the hardness of the capture  $\gamma$ -ray spectra. Since  $J = 1$  resonances exhibit substantially harder spectra, the discrepancy suggests a problem with the WF used in the previous work. A further hint in this direction is obtained from the fact that a thin sample (0.5 mm in thickness) was used in Ref. [13] for the neutron energy range

TABLE II: Resonance parameters and radiative kernels from the analysis of the  $^{207}\text{Pb}(n,\gamma)$  data measured at n\_TOF<sup>a</sup>.

$E_o$ (eV)	$l$ $J$	$\Gamma_n$ (meV)	$\Gamma_\gamma$ (meV)	$g\Gamma_\gamma\Gamma_n/\Gamma$ (meV)
3064.700(3)	1 2	111.0(8)	145.0(9)	78.6(9)
10190.80(4)	1 2	656(50)	145.2(12)	149(14)
16172.80(10)	1 2	1395(126)	275(3)	287(30)
29396.1	1 2	16000	189(7)	234(9)
30485.9(5)	1 1	608(45)	592(50)	225(30)
37751(3)	1 1	$50 \times 10^3$	843(40)	620(30)
41149(46)	0 1	$1.220 \times 10^6$	3970(160)	2970(120)
48410(2)	1 2	1000	230(20)	235(20)
82990(12)	1 2	$29 \times 10^3$	360(30)	444(30)
90228(24)	1 1	$272 \times 10^3$	1615(100)	1200(80)
127900	1 1	$613 \times 10^3$	1939(150)	1449(120)
130230	1 1	$87 \times 10^3$	900(80)	675(60)
181510(6)	0 1	$57.3 \times 10^3$	14709(500)	8780(300)
254440	2 3	$111 \times 10^3$	1219(90)	2110(150)
256430	0 1	$1.66 \times 10^6$	12740(380)	9482(280)
317000	0 1	$850 \times 10^3$	10967(480)	8120(350)

<sup>a</sup>Orbital angular momenta  $l$  and resonance spins  $J$  are from Ref. [18].

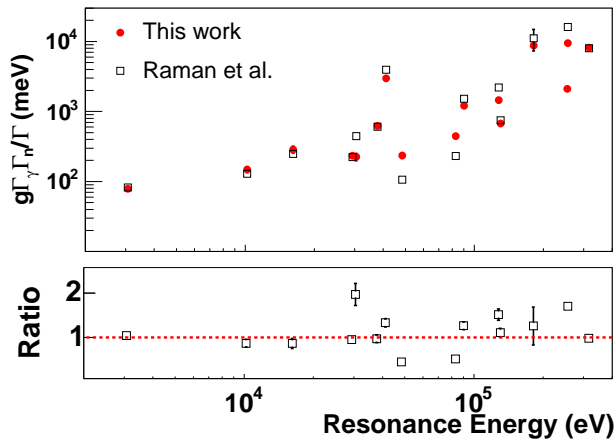


FIG. 2: (Color online) Comparison of the radiative capture kernels for  $^{207}\text{Pb}$  resonances measured at n\_TOF and ORNL [13, 14]. In the bottom panel, the ratio between the two data sets is shown.

below 45 keV, whereas a much thicker sample (16 mm) was employed above that energy. The better agreement with the thin-sample measurement suggests that the WF calculated for the analysis of Ref. [13, 14] was only valid for the thin sample case, reflecting the strong influence of the sample thickness on the shape of the WF as noted in Ref. [11].

## V. IMPLICATIONS FOR THE $s$ -ABUNDANCES IN THE PB-BI REGION

The Maxwellian averaged cross section (MACS) obtained from the present results are compared in Fig. 3 with the values reported in Ref. [19]. Within the quoted

uncertainties, both cross sections are generally in good agreement. However, the new MACSs are clearly higher at energies below  $kT = 15$  keV. In this region, the uncertainties could be reduced from 13% down to 5%, an improvement by more than a factor of two.

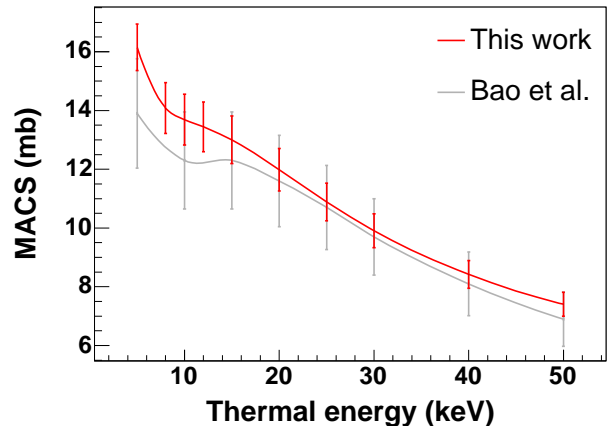


FIG. 3: (Color online) Maxwellian averaged cross sections for a range of thermal energies compared to previous values [19].

In the calculation of the MACS our results were complemented with some additional resonances from Ref. [20], which could not be observed at n\_TOF due to the in-beam  $\gamma$ -ray background. However, the contributions of these resonances are rather small, i.e. only 2% and 7% of the MACS at  $kT = 5$  and 25 keV, respectively.

TABLE III: Maxwellian averaged cross sections of  $^{207}\text{Pb}$ .

$kT$ (keV)	MACS (mb)	
	Ref. [19]	This work
5	13.9 (19)	16.2(8)
8		14.1(8)
10	12.3(16)	13.7(9)
20	11.5 (16)	12.0(7)
25	10.7 (14)	10.9(6)
30	9.7(13)	9.9(6)

According to the Galactic chemical evolution (GCE) model described in Refs. [21, 22], the  $s$ -process abundance of  $^{207}\text{Pb}$  is essentially produced in low mass asymptotic giant branch (AGB) stars. In these AGB stars energy is produced in a thin layer surrounding the inert C/O core. Subsequently, extended and quiescent H-shell burning episodes are followed by much shorter He shell flashes [23]. In this model about 95% of the neutron exposure is due to the  $^{13}\text{C}(\alpha, n)^{16}\text{O}$  reaction, which operates during the interpulse phase between He shell flashes at temperatures around  $\sim 10^8$  K, corresponding to a thermal energy of  $kT \approx 8$  keV. At this stellar temperature the present MACS is about 13% higher than the value reported in Ref. [19]. In order to estimate the effect of the higher cross section on the calculated  $s$ -process abundances, a model calculation was made for thermally pulsing AGB

stars with  $M = 3M_{\odot}$ ,  $M = 1.5M_{\odot}$  and a combination of metallicities:  $[\text{Fe}/\text{H}] = -0.3$  (most characteristic of the main  $s$  component [24]), and  $[\text{Fe}/\text{H}] = -1$  (representative of the strong  $s$  component [2, 21]). In this way, the  $s$ -process fraction of  $^{207}\text{Pb}$  could be determined as  $N_s = 77(8)\%$ , instead of  $82(18)\%$  [2]. In the present determination of  $N_s$  for  $^{207}\text{Pb}$ , the contributions obtained for the main and strong components were 60% and 17% of the solar  $^{207}\text{Pb}$  abundance, respectively. In the evaluation of the final uncertainty of the  $s$ -process abundance of  $^{207}\text{Pb}$ , the estimated contribution due to the uncertainty in its cross section is now small, of about 3%. The contribution due to the uncertainty in the neutron capture cross sections of  $^{204}\text{Pb}$ ,  $^{205}\text{Pb}$ , and  $^{206}\text{Pb}$  [19] has been estimated as less of 2%. The uncertainties of the  $s$ -process model are estimated to be  $\pm 3\%$  for the main and  $\pm 10\%$  for the strong component, resulting a contribution of less than 4% to the total uncertainty in the  $s$ -process abundance of  $^{207}\text{Pb}$ . Finally, the main source of uncertainty in the determination of  $N_s$  for  $^{207}\text{Pb}$  is due to the uncertainty in the solar abundance of lead, which is of 8-10% [25, 26, 27].

Since the  $s$  abundance of this isotope is robust with respect to uncertainties in the  $s$ -process model, the  $r$  component can now be constrained as  $N_r = 23(8)\%$ . Within the quoted uncertainty of 35%, this result is compatible with earlier  $r$ -process calculations [1] based on the ETFSI-Q nuclear mass model, which find an  $r$ -process fraction for  $^{207}\text{Pb}$  of 18.4% with an uncertainty of 10-20%, and with  $r$  abundance calculations reported more recently [28], which yield values between 15.1% and 16.4%.

## VI. CONCLUSIONS

The neutron capture cross section of  $^{207}\text{Pb}$  has been measured at the high resolution neutron time-of-flight facility n\_TOF.

The main sources of systematic uncertainty affecting this measurement have been treated in detail. From the experimental point of view background due to scattered neutrons could be eliminated by means of an optimized detection setup, and angular distribution effects were minimized by setting the detectors at  $125^\circ$  with respect to the neutron beam. In data analysis, the remaining systematic effects have been carefully corrected, resulting in a 3% accuracy for the radiative kernels of the capture resonances, except for three cases, where missing angular distribution data led to an uncertainty of 8%.

We report resonance parameters and capture areas for 16 resonances in the neutron energy interval from 3 keV to 320 keV. At low neutron energies our results are in good agreement with previous data, but reveal significant discrepancies for resonances above 40 keV. Maxwellian averaged cross sections for  $^{207}\text{Pb}$  were determined with an accuracy of  $\pm 5\%$ . With this information the  $s$ -process component of solar  $^{207}\text{Pb}$  was determined to be 77(8)%

resulting in an  $r$  fraction of 23(8)%.

## Acknowledgments

This work was supported by the EC under contract FIKW-CT-2000-00107, by the Spanish Ministry of Science and Technology (FPA2001-0144-C05) and by the funding agencies of the participating institutes. It is part of the PhD-Thesis of C.D. who acknowledges financial support from Consejo Superior de Investigaciones Cientificas.

- 
- [1] J. J. Cowan, B. Pfeiffer, K.-L. Kratz, F.-K. Thielemann, C. Sneden, S. Bures, D. Tytler, and T. C. Beers, *Astrophys. J.* **521**, 194 (1999).
- [2] U. Ratzel, C. Arlandini, F. Käppeler, A. Couture, M. Wiescher, R. Reifarh, R. Gallino, A. Mengoni, and C. Travaglio, *Phys. Rev. C* **70**, 065803 (2004).
- [3] C. Rubbia et al. (1998), CERN/LHC/98-02 (EET), CERN, Geneva.
- [4] The n\_TOF Collaboration (1999), CERN/SPSC 99-8, SPSC/P 310.
- [5] R. Plag, M. Heil, F. Käppeler, P. Pavlopoulos, R. Reifarh, K. Wisshak, and The n\_TOF Collaboration, *Nuclear Instruments and Methods in Physics Research A* **496**, 425 (2003).
- [6] C. Domingo-Pardo, U. Abbondanno, G. Aerts, H. Álvarez-Pol, F. Alvarez-Velarde, S. Andriamonje, J. Andrzejewski, P. Assimakopoulos, L. Audouin, G. Badurek, et al., *Phys. Rev. C* **74**, 025807 (2006).
- [7] S. Marrone, P. F. Mastinu, U. Abbondanno, R. Bacconi, E. B. Marchi, N. Bustreo, N. Colonna, F. Gramegna, M. Loriggiola, S. Marigo, et al., *Nuclear Instruments and Methods in Physics Research A* **517**, 389 (2004).
- [8] R. Macklin and J. Halperin, *Phys. Rev. C* **14**, 1389 (1976).
- [9] C. Domingo-Pardo (2005), Ph.D. Thesis, CSIC-University of Valencia.
- [10] PTB group (2002), n\_TOF neutron fluence with the PTB Fission Chambers, CERN/SL/ECT/2002.
- [11] J.L. Tain et al., *J. Nucl. Sci. Techn. Suppl.* 2 p. 689 (2002).
- [12] U. Abbondanno, G. Aerts, H. Alvarez, S. Andriamonje, A. Angelopoulos, P. Assimakopoulos, C. O. Bacri, G. Badurek, P. Baumann, F. Bečvář, et al., *Nuclear Instruments and Methods in Physics Research A* **521**, 454 (2004).
- [13] S. Raman, M. Mizumoto, and R. L. Macklin, *Physical Review Letters* **39**, 598 (1977).
- [14] S. Raman, M. Mizumoto, G. G. Slaughter, and R. L. Macklin, *Physical Review Letters* **40**, 1306 (1978).
- [15] C. D. Bowman, R. J. Baglan, B. L. Berman, and T. W. Phillips, *Physical Review Letters* **25**, 1302 (1970).
- [16] A.J. Ferguson, *Angular correlation methods in gamma-ray spectroscopy* (North-Holland Publishing Company-Amsterdam, 1965).
- [17] N. Larson (2000), SAMMY: Multilevel R-matrix fits to neutron data using Bayes equations, ORNL/TM-9179.
- [18] S.F. Mughabghab (1984), *Neutron Cross Sections: Neutron Resonance Parameters and Thermal Cross Sections*, Academic press.
- [19] Z.Y. Bao et al. (2000), *At. Data Nucl. Data Tables* **76**, 70.
- [20] S.I. Sukhoruchkin, Z.N. Soroko and V.V. Deriglazov (1998), *Low Energy Neutron Physics, Volume I/16B, Tables of Neutron Resonance Parameters* (Springer, Landolt-Börnstein).
- [21] C. Travaglio, D. Galli, R. Gallino, M. Busso, F. Ferrini, and O. Straniero, *Astrophys. J.* **521**, 691 (1999).
- [22] C. Travaglio, R. Gallino, M. Busso, and R. Gratton, *Astrophys. J.* **549**, 346 (2001).
- [23] R. Gallino, C. Arlandini, M. Busso, M. Lugaro, C. Travaglio, O. Straniero, A. Chieffi, and M. Limongi, *Astrophys. J.* **497**, 388 (1998).
- [24] C. Arlandini, F. Käppeler, K. Wisshak, R. Gallino, M. Lugaro, M. Busso, and O. Straniero, *Astrophys. J.* **525**, 886 (1999).
- [25] E. Anders and N. Grevesse, *Geochimica et Cosmochimica Acta* **53**, 197 (1989).
- [26] K. Lodders, *Astrophys. J.* **591**, 1220 (2003).
- [27] M. Asplund, N. Grevesse, and A. J. Sauval, in *ASP Conf. Ser. 336: Cosmic Abundances as Records of Stellar Evolution and Nucleosynthesis*, edited by T. G. Barnes, III and F. N. Bash (2005), pp. 25–+.
- [28] K.-L. Kratz, B. Pfeiffer, J. J. Cowan, and C. Sneden, *New Astronomy Review* **48**, 105 (2004).